
Observing the Gravity Field of Different Planets and Moons by Space-Borne Techniques: Predictions by Fast Error Propagation Tools

P.N.A.M. Visser

Abstract

In the first decade of the twenty first century, great strides have been made in observing the Earth's gravity field by space-borne techniques such as high-low Satellite-to-Satellite tracking by the Global Positioning System (hl-SST, providing 3D information about orbit perturbations), low-low Satellite-to-Satellite tracking (ll-SST) and Satellite Gravity Gradiometry (SGG). In addition, great advances have been made in (preparations for) gravity field recovery for other bodies in the solar system as well, including Mars and the Moon, using tracking from the Deep Space Network (DSN), but also techniques such as hl-SST, ll-SST, Satellite Laser Ranging (SLR) and Delta VLBI.

The purpose of the work described in this paper is to gain insight in the possibilities of observing the gravity field of various planetary bodies by space-borne observation techniques. For low-earth orbiting (LEO) satellites, efficient error propagation tools are available that allow an assessment of the gravity field performance as a function of orbital geometry and instrument or observation technique. These tools have been extended for use to other bodies in our solar system, including the Earth's Moon, Jupiter, Mars, Titan, Enceladus, Europa and Phobos, which are in the scientific spotlight for various reasons. The gravity field performance has been assessed for satellites orbiting these bodies assuming these satellites can make use of DSN tracking or can acquire ll-SST or SGG observations.

Keywords

Error propagation tools • Moons • Planets • Space-borne gravimetry

1 Introduction

In the past decade, significant advances have been made in the observation, modeling and interpretation of not only the gravity field of the Earth, but also of other celestial bodies in the solar system. For the Earth, continuous three-dimensional (3D) tracking in combination with a high-precision accelerometer allowed for the first time the derivation of homogeneous gravity field models for medium to long wavelengths (CHAMP, Reigber et al. 1999). The

addition of low-low Satellite-to-Satellite tracking, or ll-SST, enabled the observation of temporal gravity variations (GRACE, Tapley and Reigber 1999). Finally, using a space-borne gradiometer further enhanced the observation of Earth's gravity field down to spatial scales of 100 km and below (GOCE, Drinkwater et al. 2007).

Also for other celestial bodies such as the Earth's Moon and Mars already significant gravity field information has been extracted by analyzing DSN—and for the Moon also hl-SST, Satellite Laser Ranging (SLR) and VLBI—tracking to—or by—missions such as Clementine, Lunar Prospector, LRO, SELENE and Mars Global Surveyor (Smith et al. 2009; Matsumoto et al. 2010). Major improvements can be expected from the GRAIL mission, which—like GRACE—makes use of the ll-SST technique. Due to the absence

P.N.A.M. Visser (✉)
Faculty of Aerospace Engineering, Delft University of Technology,
Kluyverweg 1, 2629 HS Delft, The Netherlands
e-mail: P.N.A.M.Visser@tudelft.nl

of a (significant) atmosphere, the GRAIL satellites will fly very low at the end of their mission possibly allowing the construction of a gravity field model with a spatial resolution of 10 km (NASA 2012a).

In addition, DSN tracking of *e.g.* the Galileo and Cassini/Huygens missions during their encounters with the icy moons Europa and Titan allowed for the retrieval of gravity field information, be it rather coarse, which helps to reveal secrets about their internal structure (Iess et al. 2010; Rappaport et al. 2008). It is interesting to note that especially SLR techniques are progressing fast allowing tracking of very remote satellites (*cf.* the MESSENGER mission to Mercury, Smith et al. 2006).

It is fair to conclude that precise and detailed knowledge of the gravity field of celestial bodies is essential for revealing and understanding their internal structure and composition, and also for applications such as mission operations. A number of spaceborne techniques, including hl-SST, ll-SST and gradiometry are at our disposal for determining the gravity field of not only Earth, but also for example the Moon. Recent technological developments, such as Micro-ElectroMechanical systems (MEMS) based accelerometers and possibly gradiometers, might lead to miniaturized instruments that are feasible for future missions to other celestial bodies in our solar system (Flokstra et al. 2009). Therefore, it is interesting to consider and study future mission scenarios for determining the gravity field of these bodies. Detailed concept studies and full-scale simulations of for example high degree and order gravity field recovery using spaceborne gravimetry are time consuming and require significant computing resources. Fortunately, efficient error propagation tools exist and have been used as a first step for designing gravity field satellite missions for the Earth (Colombo 1984; Rosborough 1987; Visser 2005), thereby reducing the search space and limiting the number of satellite missions that are interesting for detailed and comprehensive further study. It is interesting to note that the match between error predictions by these tools and actual performance is quite close for a mission like the European Space Agency GOCE satellite, for which detailed observation error models were available (ESA 1999; Pail et al. 2011). The tools can be used in the early design phases of gravity field satellite missions to other celestial bodies as well. This paper contains results for a selection of observation techniques, a selection of celestial bodies and a selection of orbital geometries to show the potential of these tools. It has to be stressed that these results should be seen as a first step in the design process of possible gravity field missions.

This paper is organized as follows: after briefly introducing the selected planets and moons (Sect. 2), a few words will

Table 1 Selected planets and moons (*cf.* NASA 2012b)

Body	Mass (kg)	Mean equat. radius (km)	Rotation per. (Earth days)
Earth	5.9722×10^{24}	6,378.1	0.99727
Mars	6.4185×10^{23}	3,396.2	1.02595
Jupiter	1.8986×10^{27}	71,492.0	0.414
Moon	7.349×10^{22}	1,736.0	27.3217
Europa	4.80×10^{22}	1,569.0	3.551
Titan	1.3455×10^{23}	2,575.0	15.9454
Enceladus	1.08×10^{20}	250.0	1.3702
Phobos	10.6×10^{15}	13.4	0.31891

be spent on the methodology of the error propagation tools (Sect. 3). This will be followed by an overview of results (Sect. 4). The paper will be concluded with a short discussion (see section “Discussion and Conclusions”).

2 Planets and Moons

A limited selection of celestial bodies in the solar system has been made. The rationale between this selection is the possibility to assess the impact of different dimensions of such bodies (mass, size, but also rotation rate). For example, Jupiter is selected as an example of a giant planet and Phobos as an example of a very small moon. The other selected bodies more or less fill the range between these two extremes (Table 1).

For all the selected bodies, the retrieval of (more detailed) gravity information is valuable to address interesting scientific issues. The Earth speaks for itself. For Mars, gravity field information is crucial for *e.g.* analyzing the nature of the Tharsis region (Boyce 2008). For Jupiter, more information about its gravity field will help to learn more about its internal structure (Guillot et al. 2004). The Moon is interesting as non-hydrostatic (or isostatically uncompensated) components of its gravity field are relatively large (Bills and Lemoine 1995). More detailed gravity field information is required for drawing final conclusions about the existence of *e.g.* (subsurface) oceans on the icy moons Europa and Titan (Anderson et al. 1998; Rappaport et al. 2008; Iess et al. 2010), and also Enceladus (Porco et al. 2006). Finally, precise measurements of the gravity field of Phobos will help to put new constraints on the origin of this small moon of Mars (Rosenblatt et al. 2011). Please note many more questions and also many applications can be mentioned. This paragraph is however not intended to be complete and just serves to exemplify the importance of gravity field information.

3 Methodology

The error propagation tools provide estimates of the precision of spherical harmonic (SH) coefficients representing the gravity field potential of the celestial body of interest. It might be argued that SH coefficients are not the most efficient representation form for all celestial bodies, especially those with a very irregular shape (*e.g.* Phobos). However, because of the computational efficiency of the error propagation tools, it is feasible to use even very high degree and order SH expansions and thus predict the performance for small spatial structures or features if so required. The SH coefficient error estimates are based on the inverse of the normal equations that result from a least-squares estimation process that takes into account the choice of observation technique, orbital geometry and measurement error spectrum, possibly frequency dependent (see *e.g.* Schrama 1991). In case of a circular repeat orbit (most planetary orbiters fly in near-circular orbits, especially gravity field satellites) and constant measurement time interval, it can be proved that the normal matrix becomes block-diagonal when organized per SH order. In addition, it can be proved that even and odd parities of SH coefficients are uncorrelated (Colombo 1984). The maximum size of the matrix blocks that have to be inverted is therefore equal to about half the maximum SH degree (Colombo 1984). It has to be mentioned that for this specific block-diagonal structure of the normal matrix, one more condition has to be met: the number of orbital revolutions in the repeat period has to be larger than twice the maximum SH degree. On a typical standard PC (cost around €1,000 in October 2012), about 10 s CPU time is required per mission scenario for an error estimate up to degree and order 150.

Furthermore, the method of error propagation requires the establishment of transfer functions that establish the relationship between SH coefficients and the observations in the frequency domain. For this paper, the considered observation techniques are hl-SST, ll-SST and SGG. For the first two techniques use is made of a linearized orbit perturbation theory. For SGG, which can be considered an in-situ observation technique, a direct linear relationship exists with the SH coefficients. The transfer functions for orbit perturbations, ll-SST and SGG have been derived, and their validity shown, by several authors (see *e.g.* Colombo 1984; Rosborough 1987; Schrama 1991; Visser 2005). The last two techniques are capable of providing continuous observations with a constant time interval. For hl-SST tracking, it can be argued that for Earth orbiting satellites perturbations in 3 directions can be derived continuously with a constant time interval as well using for example tracking by the Global Positioning System (GPS). However, when relying on for example DSN tracking, this will not be the case. As a (very) rough approximation, it is therefore assumed that DSN

tracking provides continuous information about the radial velocity of the satellite (in a next step the error propagation tools might be compared and possibly calibrated by selected rigorous full-scale simulations). In case the mission duration is long enough and in case the satellite is not in phase lock with the Earth a full coverage can be obtained. For the Moon, which is in phase lock, this means that the performance assessment should be interpreted with care. In fact, it can be argued that this performance assessment then would hold for the near side only.

It has to be noted that other observation techniques might have been considered as well and the error propagation tools can easily be adapted to include those. For example, there have been a number of planetary orbiters that carried an altimeter. Associated observations also provide information about radial orbit perturbations. However, it is not straightforward to use altimeter observations directly for gravity field determination, because assumptions have to be made about how the topography of the celestial body of interest was formed (*e.g.* degree of isostatic compensation). Using altimeter crossovers is also not straightforward, since it requires a very precise positioning of the spacecraft for determining the exact crossover location and also provides a sparse global coverage (Mazarico et al. 2012).

As a baseline, for all missions to be assessed a mission duration of four Earth months has been assumed (which is a hypothetical mission duration in case of DSN tracking, for which a longer period will be required to have full global coverage). Polar orbits are taken to guarantee global coverage. The observation time interval is taken equal to 1 min. For Doppler tracking by DSN or the derived radial velocities, an integration interval of 1 min is applied as well. The assumed precision for radial velocities, ll-SST range-rates and SGG observations is taken equal to 1 cm/s, 100 $\mu\text{m/s}$ and 1 E (Eötvös Unit), respectively. The separation angle for the ll-SST observations is 1° orbital angle. Observation errors are assumed to have a Gaussian distribution. When using gravity gradiometry, it is assumed that the three diagonal components are available. Nominally, errors are estimated for a SH expansion complete to degree and order 150.

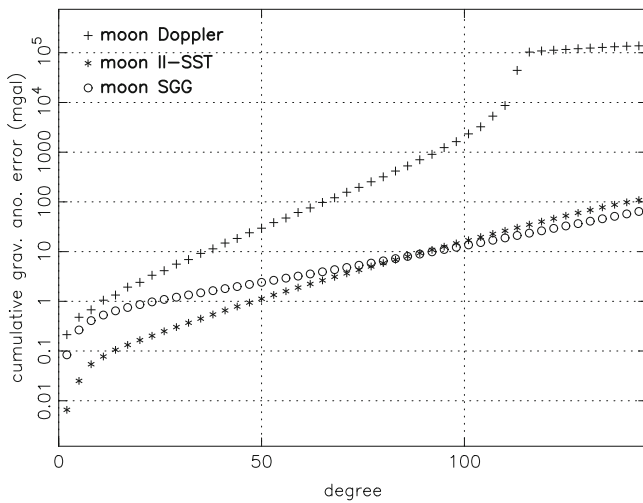
4 Results

As a first example, the lunar gravity field performance for the selected observations techniques is compared for a satellite in a polar orbit at an altitude of 73 km. Please note that this example is not to be interpreted as the possible performance by the GRAIL mission. In fact, the performance for GRAIL is expected to be much better due to the lower instrument noise ($\ll 100 \mu\text{m/s}$) and its much lower altitude (50 km and below), *cf.* MIT (2012)). The repeat period is one Lunar day or about 28 Earth days. The normal equations are scaled by

Table 2 Satellite altitudes for the investigated satellite gravity mission to the selected celestial bodies

Body	Height (km)	Repeat period		Number of repeats
		n_{rev}	$n_{bodyday}$	
Earth	265	671	42	3.0
Mars	139	568	41	3.0
Jupiter	2,965	324	103	3.0
Moon	73	341	1	4.5
Europa	69	499	12	3.0
Titan	106	1,045	7	1.0
Enceladus	11	371	31	3.0
Phobos	0.6	293	132	3.0

Please note that the repeat period is specified in terms of orbital revolutions n_{rev} and the number of planet/moon days $n_{bodyday}$, i.e. the period such a planet/moon needs to complete one revolution around its axis

**Fig. 1** Lunar gravity field performance in terms of cumulative gravity anomaly error based on Doppler, II-SST range-rate and SGG observations for a satellite altitude of 73 km

a factor of 4.5 to have a mission duration of about four Earth months (Table 2). The estimated performance is displayed in Fig. 1 in terms of cumulative gravity anomaly error. Please note that if required, the errors can also be represented in terms of other gravity field functionals, such as equipotential surface (geoid, selenoid, . . .), deflections of the vertical, etc. The shape of these curves is as anticipated: the slope is the steepest for Doppler and the least steep for SGG observations. Doppler observations represent orbit perturbations that are obtained by integration in time of the (gravitational) accelerations that the satellite experiences, whereas SGG observations are obtained by taking the difference between very adjacent, typically at a distance of 0.5 m or less, accelerations thereby enhancing shorter wavelengths. The II-SST observations represent orbit perturbation differences between two relatively nearby satellites resulting in a slope in between those of Doppler and SGG observations. Based on the curves

in Fig. 1, it might be concluded that the II-SST technique is the superior one for lunar gravity field retrieval up to degree and order 90, or a smallest spatial scale of about 60 km. For smaller spatial scales, the SGG technique displays a better performance. The Doppler technique leads to a relatively poor performance and as stated above, it can be argued that this performance is achievable only for the near side due to the phase lock of the Moon with the Earth. As also stated before, these results should be considered as an example of the capabilities of the error propagation tools as a preliminary step in the design process. The relative performance of the different techniques depends of course on the underlying assumptions that were made. For example, the error curves scale proportionally with the assumed observation noise level and signature. The chosen noise levels for all the techniques were taken at rather conservative levels. If the noise level for the II-SST is a factor 10 better, i.e. $10 \mu\text{m/s}$, the associated error curve will shift by one order of magnitude and the SH degree at which the II-SST curve intersects with the SGG one will shift to a significantly higher degree. Of course, a similar “vice-versa” reasoning can be used when reducing the noise level of SGG observations. As another example, a bandwidth limitation (i.e. high noise at low frequencies), which is typical for a gradiometer, will significantly degrade the performance for low SH degrees. Hence, the error analysis can be refined and lead to more realistic gravity field retrieval performance assessments if more information becomes available about the noise characteristics of the observation technique(s) and/or selected instruments.

The error curve for the Doppler observations displays a distinct increase around degree 115. This can be explained by considering the Doppler integration interval of 1 min. For the Lunar mission, the satellite travels a distance equal to about 3.12° in terms of orbital angle, which is around 1/115th of an orbital revolution, or the inverse of the SH degree where the jump kicks in.

As a second example, polar orbits were selected for other celestial bodies with altitudes that are scaled by the radius of the associated body of interest, i.e.:

$$\frac{a_b}{r_b} = \frac{a_e}{r_e} \quad (1)$$

where a_i and r_i represent respectively the semi-major axis of the satellite orbit and radius of the selected celestial body ($i = b$), where the Earth ($i = e$) serves as reference using an altitude of about 300 km. Please note that also other scaling rules can be applied and of course other altitudes can be selected. The scaling is applied to take into account the consideration that for smaller bodies gravity signals will dampen out faster with increasing altitude.

The scaling rule of Eq. (1) leads to different repeat orbits and associated number of orbital revolutions (Table 2), which

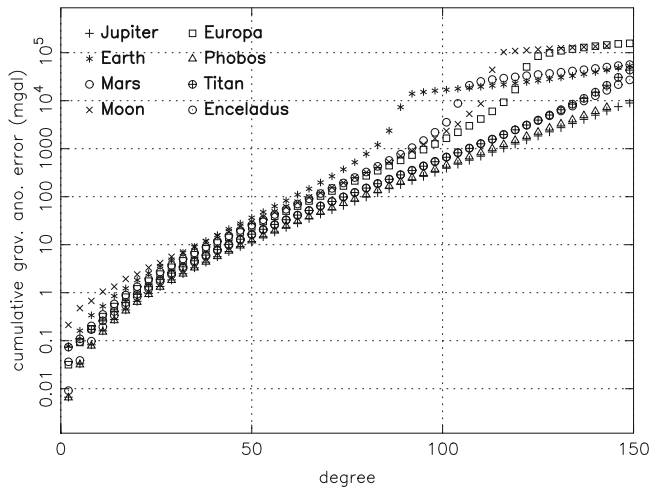


Fig. 2 Gravity field performance in terms of cumulative gravity anomaly error based on Doppler observations for scaled satellite altitudes (using a reference altitude of ≈ 300 km for the Earth)

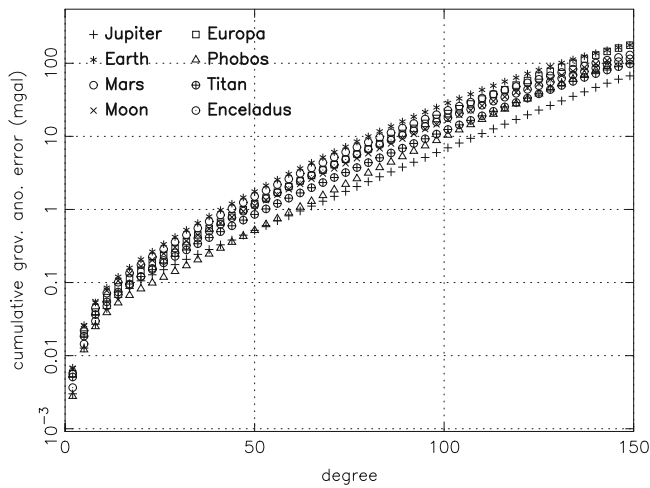


Fig. 3 Gravity field performance in terms of cumulative gravity anomaly error based on II-SST range rate observations for scaled satellite altitudes (see Fig. 2)

for all bodies, except Phobos, is above 300, i.e. formal error estimates can be obtained for SH coefficients up to degree and order 150 (140 is taken for Phobos). Different repeat periods are obtained, which is the reason for scaling the normal equations with the specified number of repeats to end up with a four Earth month observation period for all selected mission scenarios.

The gravity field performance for the several celestial bodies is displayed in Figs. 2, 3 and 4 for radial Doppler, II-SST range-rate and SGG observations, respectively, in terms of cumulative gravity anomaly error. It can be observed that curves look quite similar for the Doppler and II-SST observation techniques for SH degrees up to at least 50, for all selected celestial bodies (both the very small and big ones). For the Doppler technique (Fig. 2), jumps occur at

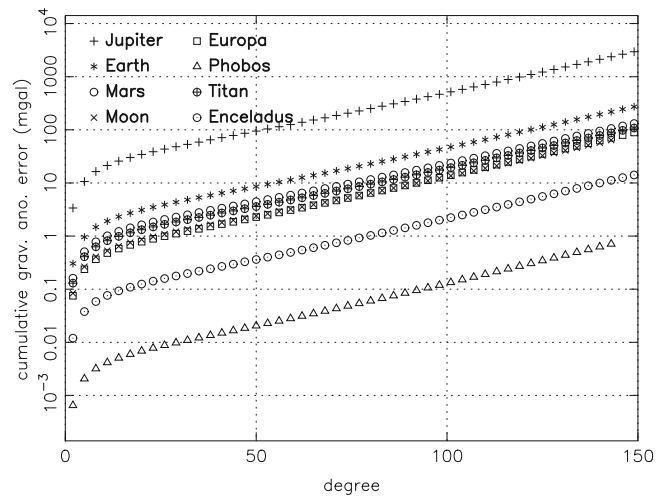


Fig. 4 Gravity field performance in terms of cumulative gravity anomaly error based on SGG observations for scaled satellite altitudes (see Fig. 2)

different SH degree which can be explained by the different rotation rates for the selected satellite orbits combined with Doppler integration interval of 1 min (see also the explanation above for the Lunar mission scenarios, Fig. 1). For the SGG observation technique, the error curves are also very similar, except for the absolute magnitude. In terms of cumulative gravity anomaly error, the errors for the largest selected planet (Jupiter) are between 3 and 4 orders of magnitude larger than for the smallest selected moon (Phobos). A preliminary conclusion might be that the SGG technique is relatively promising for small bodies. As stated before, the Doppler and II-SST observation techniques provide information about (relative) orbit perturbations, which are obtained by integration of the equations of motion or integration of the gravitational acceleration. SGG observations however are obtained by differentiation of the gravitational acceleration. By using scaled altitudes Eq. (1), the SGG technique has a natural advantage for small bodies as compared to the other techniques.

Discussion and Conclusions

Efficient error propagation tools originally used for Earth gravity field satellite missions have been adjusted to enable first assessments of gravity field retrieval performance for satellite missions to other celestial bodies. A number of space-borne gravimetry techniques have been selected to serve as example, including (hypothetical) Doppler observations of the radial velocity of the satellite, II-SST range rate observations, and SGG observations.

The gravity field retrieval performance was assessed for nominal mission scenarios, where the mission duration is equal to four Earth months and the satellites fly in polar repeat orbits. Concerning the different techniques,

results are in agreement with intuition and experience for the Earth. For Doppler tracking, the error curves have the steepest slope, i.e. gravity field retrieval errors grow relatively fast with increased spatial resolution. On the other hand for SGG observations, the slope is the smallest, i.e. the SGG technique performs relatively well at short spatial scales.

The conducted error propagation assessments described in the previous sections can be considered as a nice exercise to show the capability of the used tools for designing possible future gravity field mission to different celestial bodies in our solar system. When mission and instrument design evolve, more realistic observation error spectra can be used to improve the gravity field performance estimates. It can be stated that the error propagation tools are very flexible and can easily accommodate many observation techniques, orbital geometries and different celestial bodies. These tools provide a first quick insight into gravity field mission concepts that are feasible and can be selected for more comprehensive study.

References

- Anderson JD, Schubert G, Jacobson RA et al (1998) Europa's differentiated internal structure: inferences from four galileo encounters. *Science* 281:2019–2022
- Bills BG, Lemoine FG (1995) Gravitational and topographic isotropy of the earth, moon, mars, and venus. *J Geophys Res* 100(E12):26275. doi:10.1029/95JE02982
- Boyce JM (2008) The smithsonian book of mars Konecky & Konecky, Old Saybrook, CT, p 107. ISBN 1-56852-714-4
- Colombo OL (1984) The global mapping of gravity with two satellites. vol 7, no. 3. Netherlands Geodetic Commission, Publications on Geodesy, New Series
- Drinkwater M, Haagmans R, Muzzi D et al (2007) The GOCE gravity mission: ESA's first core explorer. In: 3rd GOCE user workshop, 6–8 November 2006, Frascati, pp 1–7. ESA SP-627
- ESA (1999) Gravity field and steady-state ocean circulation mission Reports for mission selection, The four candidate earth explorer core missions, SP-1233(1). European Space Agency (July 1999)
- Flokstra J, Cupurus R, Wiegerink RJ, van Essen MC (2009) A MEMS-based gravity gradiometer for future planetary missions. *Cryogenics* 49(11):665–668. ISSN 0011-2275
- Guillot T, Stevenson DJ, Hubbard WB, Saumon D (2004) Chapter 3: The interior of jupiter. In: Bagenal F, Dowling TE, McKinnon WB (eds) *Jupiter: the planet, satellites and magnetosphere*. Cambridge University Press, Cambridge. ISBN 0-521-81808-7
- Iess L, Rappaport NJ, Jacobson RA et al (2010) Gravity field, shape, and moment of inertia of titan. *Science* 327:1367–1369
- Matsumoto K, Goossens S, Ishihara Y et al (2010) An improved lunar gravity field model from SELENE and historical tracking data: Revealing the farside gravity features. *J Geophys Res* 115(E06007):1–20. doi:10.1029/2009JE003499
- Mazarico E, Rowlands DD, Neumann GA et al (2012) Orbit determination of the lunar reconnaissance orbiter. *J Geod* 86:193–207. doi:10.1007/s00190-011-0509-4
- MIT (2012) GRAIL Gravity recovery and interior laboratory. <http://moon.mit.edu/overview.html>. Last accessed 23 Nov 2012
- NASA (2012a) GRAIL gravity recovery and interior laboratory. http://www.nasa.gov/mission_pages/grail/main/. Last accessed 8 Oct 2012
- NASA (2012b) Lunar and planetary science. <http://nssdc.gsfc.nasa.gov/planetary>. Last accessed 25 Oct 2012
- Pail R, Bruinsma S, Migliaccio F et al (2011) First GOCE gravity field models derived by three different approaches. *J Geod* 85:819–843. doi: 10.1007/s00190-011-0467-x
- Porco CC, Helfenstein P, Thomas PC et al (2006) Cassini observes the active south pole of enceladus. *Science* 311:1393–1401. doi:10.1126/science.1123013
- Rappaport NJ, Iess L, Wahr J et al (2008) Can cassini detect a subsurface ocean in titan from gravity measurements? *Icarus* 194:711–720
- Reigber Ch, Schwintzer P, Lühr H (1999) The CHAMP geopotential mission. In: Marson I, Sünkel H (ed) *Bollettino di Geofisica Teorica e Applicata*, vol 40, no. 3–4. pp. 285–289. Istituto Nazionale di Oceanografia e di Geofisica Sperimentale - OHS, Trieste, Italy. ISSN 0006-6729
- Rosborough GW (1987) Radial, transverse, and normal satellite position perturbations due to the geopotential. *Celest Mech* 40:409–421
- Rosenblatt P, Rivoldini A, Rambaux N, Dehant V (2011) Mass distribution inside Phobos: a key observational constraint for the origin of Phobos. In: EPSC Abstracts, vol 6, EPSC-DPS2011-761, EPSC-DPS Joint Meeting 2011
- Schrama EJO (1991) Gravity field error analysis: Applications of global positioning system receivers and gradiometers on low orbiting platforms. *J Geophys Res* 96(B12):20041–20051
- Smith DE, Zuber MT, Sun X et al (2006) Two-way laser link over interplanetary distance. *Science* 311(53). doi: 10.1126/science.1120091
- Smith DE, Zuber MT, Torrence MH et al (2009) Time variations of Mars' gravitational field and seasonal changes in the masses of the polar ice caps. *J Geophys Res* 114(E05002):1–15 doi:10.1029/2008JE003267
- Tapley BD, Reigber Ch (1999) GRACE: A satellite-to-satellite tracking geopotential mapping mission. In: Marson I, Sünkel H (eds) *Bollettino di Geofisica Teorica e Applicata*, vol 40, no 3–4, p 291. Istituto Nazionale di Oceanografia e di Geofisica Sperimentale - OHS, Trieste, Italy. ISSN 0006-6729
- Visser PNAM (2005) Low-low satellite-to-satellite tracking: Applicability of analytical linear orbit perturbation theory. *J Geod* 79(1–3):160–166